

ORIGINAL ARTICLE

Intranodal delivery of modified docetaxel: Innovative therapeutic method to inhibit tumor cell growth in lymph nodes

Ariunbuyan Sukhbaatar^{1,2}  | Shiro Mori^{1,2,3} | Tetsuya Kodama^{1,2,4} 

¹Laboratory of Biomedical Engineering for Cancer, Graduate School of Biomedical Engineering, Tohoku University, Sendai, Miyagi, Japan

²Biomedical Engineering Cancer Research Center, Graduate School of Biomedical Engineering, Tohoku University, Sendai, Miyagi, Japan

³Department of Oral and Maxillofacial Surgery, Tohoku University Hospital, Sendai, Miyagi, Japan

⁴Department of Electronic Engineering, Graduate School of Engineering, Tohoku University, Sendai, Miyagi, Japan

Correspondence

Tetsuya Kodama, Laboratory of Biomedical Engineering for Cancer, Graduate School of Biomedical Engineering, Tohoku University, 4-1 Seiryō, Aoba, Sendai, Miyagi 980-8575, Japan.
Email: kodama@tohoku.ac.jp

Funding information

JSPS KAKENHI, Grant/Award Number: 18H03544, 17K20077, 17H00865, 19K22941, 21K18319 and 20H00655

Abstract

Delivery of chemotherapeutic agents into metastatic lymph nodes (LNs) is challenging as they are unevenly distributed in the body. They are difficult to access via traditional systemic routes of drug administration, which produce significant adverse effects and result in low accumulation of drugs into the cancerous LN. To improve the survival rate of patients with LN metastasis, a lymphatic drug delivery system (LDDS) has been developed to target metastatic LN by delivering chemotherapy agents into sentinel LN (SLN) under ultrasound guidance. The LDDS is an advanced method that can be applied in the early stage of the progression of tumor cells in the SLN before tumor mass formation has occurred. Here we investigated the optimal physicochemical ranges of chemotherapeutic agents' solvents with the aim of increasing treatment efficacy using the LDDS. We found that an appropriate osmotic pressure range for drug administration was 700–3,000 kPa, with a viscosity < 40 mPa·s. In these physicochemical ranges, expansion of lymphatic vessels and sinuses, drug retention, and subsequent antitumor effects could be more precisely controlled. Furthermore, the antitumor effects depended on the tumor progression stage in the SLN, the injection rate, and the volumes of administered drugs. We anticipate these optimal ranges to be a starting point for developing more effective drug regimens to treat metastatic LN with the LDDS.

KEYWORDS

docetaxel, drug delivery, lymph node metastasis, osmotic pressure, viscosity

1 | INTRODUCTION

Lymph node (LN) metastasis is one of the most salient prognostic factors for many types of cancer. Despite recent advances in the treatment of metastasis, the 5-year survival rate of patients remains poor, particularly for head and neck cancer, with average 5-year survival rates of approximately 77%, 52%, and 35% for patients with local, regional LN, and distant sites exhibiting metastases, respectively.

Thus, the prognosis is worse for patients with LN metastases than for those patients with only localized tumors.^{1,2} Survival rates depend on the stage of the cancer metastasis and are mostly correlated with the numbers of LN containing metastases. Therefore, controlling the regional LN is extremely important. Intravenous (i.v.) administration of chemotherapeutic agents is widely used for the treatment of metastatic LN. Most small molecule drugs (<10 nm) have poor aqueous solubility, low bioavailability, and little tissue selectivity.³ In addition,

This is an open access article under the terms of the Creative Commons Attribution-NonCommercial License, which permits use, distribution and reproduction in any medium, provided the original work is properly cited and is not used for commercial purposes.

© 2022 The Authors. *Cancer Science* published by John Wiley & Sons Australia, Ltd on behalf of Japanese Cancer Association.

drugs leak from blood capillaries into the interstitium and are subsequently absorbed by the lymphatic system and then reabsorbed into the blood vascular system because the lymphatic molecular absorption windows are 10–100 nm^{4,5}; an optimal range is 20–50 nm.^{6,7}

A two-stage approach to maximize drug delivery to the LN was inspired by the trafficking route of particulate antigens.⁸ After intradermal injection of approximately 27-nm diameter nanoparticles, they were transported from the interstitial space to downstream LN²⁻⁴ and accumulated there.^{6,9} Access of drugs to the lymphatic network is dependent on their molecular size^{6,8,10,11}; the LN sinus allows entry of small molecules (3–5 nm in diameter) with molecular weights <70 kDa.^{10,12-14} To increase lymphatic uptake and LN exposure, various approaches have been adopted to deliver lipid-like macro or nanoparticles interstitially or orally associated with sized colloidal lipoproteins in absorptive cells.^{6,10,11,13,15,16} However, these administration routes provide access only to the downstream LN. For diseases associated with multiple LN or LN that are not accessible by injection, delivery of therapeutic agents is challenging.

LNs are organs rich in vascular networks;¹⁷⁻¹⁹ therefore, tumor cells that have metastasized to LN can proliferate by replacing parenchyma with tumor cells but without inducing tumor neovascularization at an early stage (i.e., formation of a perfusion defect).²⁰⁻²³ Thus, the effect cannot be relied upon to deliver macromolecular drugs during the early stage of LN metastasis.²² Therefore, there is an urgent need to develop new ways to treat tumor cells in LN independent of hematogenous delivery. One potential approach is to deliver drugs directly through the lymphatic system. However, this approach cannot be readily verified in wild-type mice for two main reasons. First, the lymphatic system in mice is not easily visualized by the naked eye, partly because the LN are 1–2 mm in size and may be obscured by adipose tissue and partly because the lymphatic vessels are transparent. Second, at present, there is no reproducible LN metastasis model that can accurately predict the timing of the development of LN metastasis, excluding our MXH10/Mo/lpr mouse model. Even if metastasis is induced in LN in these mice, the metastatic LN exhibit extranodal invasion or parenchyma replacement by tumor cells during the early stage of nodal metastasis due to the small sizes of the LN.²⁴

Therefore, we established MXH10/Mo-lpr/lpr (MXH10/Mo/lpr), a recombinant inbred mouse that develops systemic swelling of LN that enlarge to 10 mm in diameter (equivalent size to LN in the human)²⁵ from 2 months of age due to the accumulation lpr-T cells (CD4⁺CD8⁺B220⁺Thy⁺).²⁶ Focusing on the positional relationship between the upstream and downstream LN in the mouse lymphatic network, we developed a reproducible LN metastatic mouse model by inoculating tumor cells into the upstream LN so that the tumor cells were directed to the downstream LN via the lymphatic vessels.^{27,28}

The aim was to increase treatment efficacy with higher delivery of particles or chemotherapeutic agents into the lymphatic system using a one-stage approach, based on the knowledge that the lymphatic network is further controlled by its anatomical structure.^{10,12,14} We used the mouse model to develop a lymphatic drug delivery system (LDDS)²⁹ that could treat sentinel LN (SLN) and their

downstream LN at the early stage of metastasis. This is achieved by the local injection of chemotherapy drugs into the SLN under ultrasound guidance or during intraoperative or image-guided surgery. Specifically, the LDDS can be used to administer chemotherapy drugs at the early stage of tumor cell spread through the lymphatic network and, therefore, inhibit distant metastasis induced by LN-mediated hematogenous metastasis theory. The advantages of the LDDS compared with other conventional cancer metastasis chemotherapy routes are extensive, such as the use of much lower concentrations of drugs and minimal side effects. The upstream and downstream LN are connected by lymphatic vessels, and the lumens of the lymphatic vessels have semilunar valves that prevent regurgitation from upstream to downstream flows.³⁰ In the LDDS, since there is no driving force (i.e., the blood circulatory system), the pressure difference between upstream and downstream flows caused by injecting the drug into the upstream LN opens the semilunar valve in the lymphatic vessel, which is then directed toward the downstream LN. When the drug is delivered in one direction and the pressure difference disappears, the drug is retained in the lymphatic network for a long time by the semilunar valve. This hydrodynamic property has never before been utilized in the current drug delivery system but confers a very important advantage for the treatment of LN metastasis.³⁰ The flow pattern differs from the normal physiological flow because of the synchronization of the lymphatic contraction and semilunar valve opening.^{31,32} In experiments using the LDDS to administer chemotherapeutic drugs (CDDP or 5-FU) at an early stage of LN metastasis, the drug dose required to produce an antitumor effect in the metastatic LN was much smaller than that needed for systemic chemotherapy.³²⁻³⁵ Furthermore, plasma biochemistry showed no evidence of acute renal failure, acute pancreatitis, or liver dysfunction when such low doses were used. Thus, it is believed that drug administration using the LDDS will produce little risk of adverse side effects yet will be a highly effective antitumor treatment.³²⁻³⁵ The results indicated that the LDDS was effective in suppressing tumor growth in metastatic LN compared to conventional hematogenous (systemic) chemotherapeutic agent treatment. The pathological analysis, however, revealed that cells growing densely in the lymphatic sinus were not markedly affected, suggesting that the lymph sinus was occluded by the presence of multiple tumor cells. In other words, the drug was not delivered around the tumor.^{32,33}

Preliminary studies have shown that physicochemical ranges were determined by two independent factors: osmotic pressure and viscosity for LDDS.³⁶ In the present study, we hypothesized that when a chemotherapeutic agent solution with high osmotic pressure and viscosity was given through the LDDS, expansion of lymphatic vessels and sinuses, drug retention, and the subsequent antitumor effect could be controlled. When tumor cells proliferate in the lymphatic sinuses, tumor embolism occurs in the lymphatic sinuses. Even if the drug reaches the lymphatic vessels from the upstream LN, the drug is not delivered due to embolization. However, increasing the osmotic pressure of the solvent of chemotherapy drugs to a certain level increased the amount of fluid stored in the lymphatic sinuses

and dilated the lymphatic sinuses, thus creating gaps between the tumor and endothelium of the lymphatic sinus. We used docetaxel (DTX) as the chemotherapeutic agent because the osmotic pressure and viscosity varied by changing the solvent's concentration, which allowed us to establish an optimal osmotic pressure and viscosity range for use with the LDDS. Furthermore, we found that the anti-tumor effects depended on the LN's tumor progression stage, the injection rate, and the volume administered. We anticipate these optimal ranges to be a starting point for the development of more effective drugs to treat metastatic LN using the LDDS. The results are considered applicable to most chemotherapeutic agent solutions and are expected to guide drug design for the LDDS.

2 | MATERIALS AND METHODS

2.1 | Solutions

Two types of solutions were prepared: 12 test solutions (A-L, Table S1) and four DTX solutions (Table S4). The 12 test solutions consisted of polysorbate 80 (NOF), 100% ethanol (Fuji Film Wako Pure Chemical), distilled water, and 0.5 mg/mL of indocyanine green (ICG, Daiichi-Sankyo). Four DTX solutions were prepared using DTX (Sanofi K. K), polysorbate 80 (NOF), 100% ethanol (Fuji Film Wako), saline (Otsuka Pharmaceutical Factory), distilled water, and 0.5 mg/mL of ICG (Daiichi-Sankyo). For the control group, polysorbate 80 was used instead of DTX. The final concentration of ICG for both solutions was 100 µg/mL. Osmotic pressure Π was calculated using the following equation:

$$\Pi = CRT, \quad (1)$$

where C denotes the molar concentration, R denotes the ideal gas constant, and T denotes the absolute temperature. The viscosity (μ) of each solution was measured by two tuning-fork vibration viscometers (SV-1H and SV-1A, A & D) at room temperature (25.6–25.8°C).

2.2 | Animal models

Animal experimental procedures were conducted in compliance with the Institutional Animal Care and Use Committee of Tohoku University's approved guidelines. MXH10/Mo-*lpr/lpr* (MXH10/Mo/*lpr*) mice (aged 16–18 weeks)^{25,32} and MXH51/Mo-*lpr/lpr* (MXH51/Mo/*lpr*) (aged 16–20 weeks)^{32,37} were housed at the Animal Research Institute, Tohoku University under specific pathogen-free conditions. MXH10/Mo/*lpr* and MXH51/Mo/*lpr* mice are remarkable in that their peripheral LN enlarge to 10 mm in size when they are 2.5 to 3 months old, and furthermore, they do not develop severe autoimmune disorders. To allocate the right anatomical positions and nomenclatures to murine LN, we used the term "subiliac LN (SiLN)" instead of "inguinal LN" and "proper axillary LN (PALN)" instead of "axillary LN".^{25,32,38}

2.3 | Determination of optimized osmotic pressure/viscosity ranges for lymphatic drug delivery system

To evaluate the effects of the viscosity and osmotic pressure of the solvent on the delivery and the sustainability of delivered drug to the targeted downstream LN using the LDDS, the 12 test solutions (Table S1) were administered into the subiliac LN (SiLN), to be delivered to the downstream LN, proper axillary LN (PALN) of each mouse. Using a 27-G butterfly needle and syringe pump, 200 µL of solution was administered into the SiLN at a rate of 10 µL/min. The fluorescence from ICG was measured using an *in vivo* imaging system (IVIS; PerkinElmer Waltham, MA, USA) on day 0 (before and after test solution injections) and on days 1, 7, 14, and 21 post-injection.^{27,32,33}

2.4 | Tumor cell implantation into the SiLN

As previously stated, all *in vivo* experiments were carried out on mice under general anesthesia (2.5% isoflurane in oxygen), and great care was taken to reduce animal suffering.^{32,39–42} The day on which the SiLN was inoculated with tumor cells was defined as day 0^I (Data S1).

2.5 | Administration of docetaxel solutions to the SiLN and PALN within optimized osmotic pressure/viscosity ranges

Experiments were divided into two types: (1) evaluation of anti-tumor effects within optimized osmotic pressure/viscosity ranges; and (2) assessment of the injection rates and volumes of DTX solution introduced into the SiLN within optimized osmotic pressure/viscosity ranges. In Group 1, mice were randomly divided into six groups: (1,140 kPa, 4 mPa·s, control, $n = 6$), (1,140 kPa, 4 mPa·s, DTX, $n = 7$), (1,960 kPa, 12 mPa·s, control, $n = 6$), (1,960 kPa, 12 mPa·s, DTX, $n = 6$), (2,780 kPa, 38 mPa·s, control, $n = 6$), (2,780 kPa, 38 mPa·s, DTX, $n = 6$), and (695 kPa DTX *i.v.*, 2 mPa·s, control, $n = 6$), as shown in Table S4. Injection of DTX solution (200 µL) into the SiLN was carried out manually with a 27-G injection needle on day 7 after inoculation day 7^I. The day in which DTX solution was injected into the SiLN was defined as day 0^T. The concentration of DTX per mouse was 10 mg/kg when the body weight was assumed to be 40 g. In Group 2, mice were divided into two treatment groups: treatment day 7^I (day 7 after inoculation) and treatment day 21^I (day 21 after inoculation). Each group was divided into four subgroups that received DTX at different injection rates and volumes: (200 µL, 200 µL/min, $n = 6$), (400 µL, 200 µL/min, $n = 6$), (200 µL, 2,400 µL/min, $n = 6$), and (400 µL, 2,400 µL/min, $n = 6$). Injection of the solution (1,140 kPa, 4 mPa·s) into the SiLN was carried out through a 27-G injection needle driven by a syringe pump. The injection rate of 2,400 µL/min was similar to that of a manual injection rate. The concentration of DTX per mouse was 10 mg/kg for a 200-µL injection and 20 mg/kg for a

400 μL injection, respectively. For assessment of tumor growth in the SiLN and PALN in the two groups, luciferase activity was measured. In the tumor growth observation groups, luciferase activity was measured on day 7^I for the D7^I group and on days 7^I, 14^I, and 21^I for the day 21^I group. Treatment days were defined as 0^T. In Group I, luciferase activity was measured on 0^T (before treatment), 3^T, 6^T, and 9^T. In Group II, luciferase activity was measured on days 0^T (before treatment), 3^T, 6^T, and 9^T for the day 7^I and day 21^I treatment groups. On every experimental day, 10 min after post-intraperitoneal administration of luciferin (150 mg/kg; Promega, Madison, WI, USA), luciferase activity was measured. SiLN and PALN volumes were measured using a high-frequency ultrasound imaging system (VEVO770, FUJIFILM VisualSonics) with a 25 MHz transducer (RMV-710B; Visual Sonics) on days 0^I (before tumor cell inoculation) and 7^I (0^T before treatment) for the day 7^I group and on days 0^I, 7^I, 14^I, and 21^I (0^T before treatment) for the day 21^I group, then on 3^T, 6^T, and 9^T for Group 1 and Group 2. The step size between each B-mode slice was 0.1 mm, and the field of view was set to 12 \times 12 mm. Values were normalized to those on day 0^I (before inoculation) to obtain normalized volume values.

3 | RESULTS

3.1 | Optimized osmotic pressure and viscosity ranges for lymphatic drug delivery system delivery

The concept of the LDDS is that a drug can be administered into the sentinel LN (SLN) or the upstream LN of a latent metastatic LN to treat the SLN and its downstream LN. To optimize the ranges of the osmotic pressure and viscosity of the solvent that are effective for the LDDS, we used polysorbate 80 and prepared test solutions adjusted to 12 levels of osmotic pressure and viscosity, as shown in Table S1 (Solution A: 1 kPa, 1 mPa-s; Solution B: 588 kPa, 1 mPa-s; Solution C: 695 kPa, 2 mPa-s etc.). Test solutions A (1 kPa, 1 mPa-s), B (588 kPa, 1 mPa-s), E (1740 kPa, 6 mPa-s), K (3481 kPa, 427 mPa-s), and L (5221 kPa, 8020 mPa-s) were administered to the SiLN, and the flow dynamics of the solutions from the SiLN to the PALN were visualized by biofluorescence imaging. The retention of each solution in the SiLN and PALN was measured before treatment (BT) and up to day 21 after treatment (AT) (Figure 1a). Each solution flowed from the SiLN into the PALN

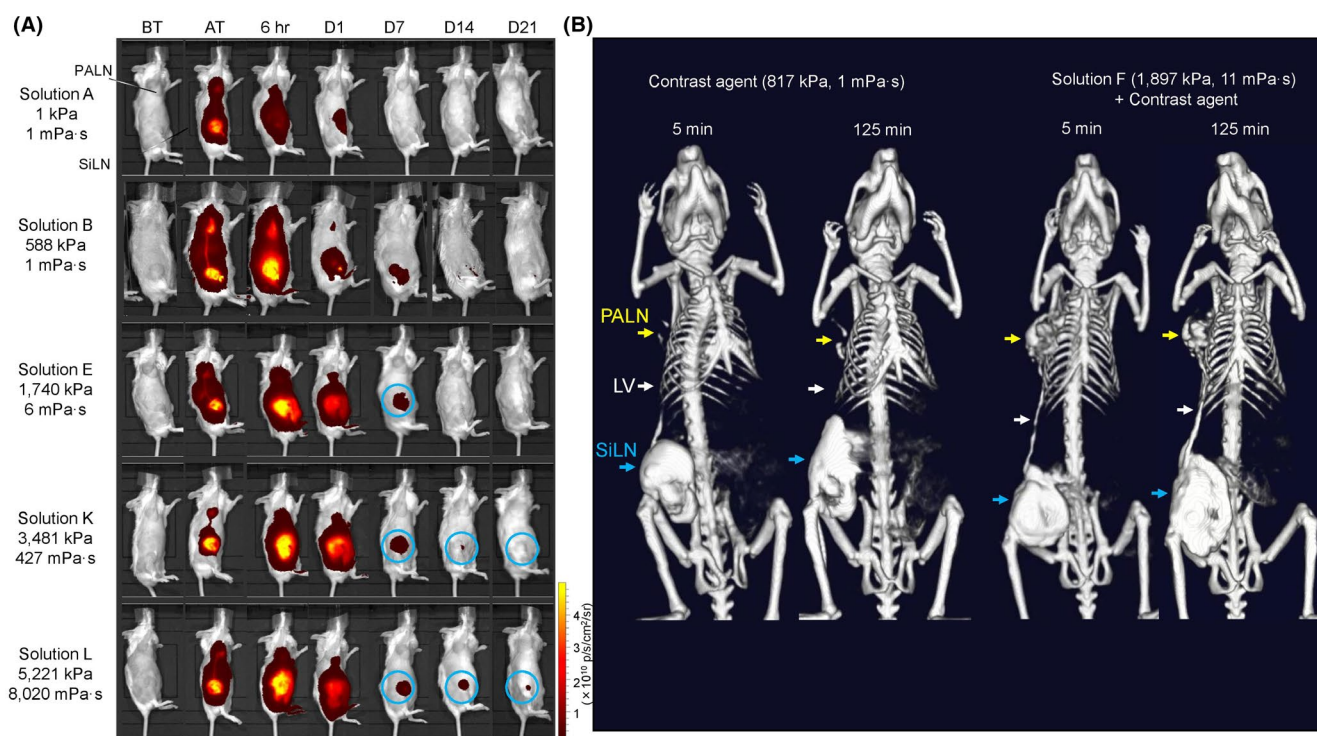


FIGURE 1 Determination of optimized osmotic pressure/viscosity ranges for lymphatic drug delivery system. (a) Two-hundred microliters of test solutions (A, B, E, K, L) were injected into the subiliac lymph nodes (SiLN) toward the proper axillary lymph nodes (PALN) at an injection rate of 10 $\mu\text{L}/\text{min}$. Fluorescence from indocyanine green (ICG) was measured with an *in vivo* biofluorescence imaging system. All solutions reached the PALN from the SiLN. The solution retention in the SiLN increased with increasing osmotic pressure and viscosity. Solutions E, K, and L induced edema in the SiLN, as indicated by circles. The onset of edema induced by solution C was shorter than that of solutions K and L. Solution A (II: 1 kPa, μ : 1 mPa-s, $n = 4$), Solution B (II: 588 kPa, μ : 1 mPa-s, $n = 4$), Solution E (II: 1,740 kPa, μ : 6 mPa-s, $n = 4$), Solution K (II: 3,481 kPa, μ : 427 mPa-s, $n = 4$), Solution L (II: 5,221 kPa, μ : 8,020 mPa-s, $n = 4$). (b) Two-hundred microliters of test solution (F) were injected into the SiLN toward the PALN at a rate of 10 $\mu\text{L}/\text{min}$, and the contrast agent was injected 5 min afterwards as a bolus. Lymphatic vessel (LV) expansion was evaluated by micro-CT for 125 min after the contrast agent injection at 5-min intervals. LV expanded in the solution F group, and this expansion increased with time. Contrast agent (II: 817 kPa, μ : 1 mPa-s, $n = 1$), solution F (II: 1987 kPa, μ : 11 mPa-s, $n = 4$) + contrast agent. (Yellow arrow, PALN; white arrow, LV; and blue arrow, SiLN)

and was drained from the SiLN and PALN, as measured by their time profiles. There were significant differences in the fluorescent intensities among the solutions each day, except immediately after treatment and on day 14. The retention of the solution in the PALN for >1 day after treatment was confirmed using solution B data (Figure 1a, Figure S1). Macroscopic observations confirmed edema that lasted for up to 7 days after solution E delivery and 21 days for K and L (Figure 1). Statistical significance was not confirmed for body weight loss associated with the administration of solutions A, B, E, K, and L (Table S2). Due to their high viscosities, it was difficult to inject solutions K (3,481 kPa, 427 mPa-s) and L (5,221 kPa, 8,020 mPa-s) into the SiLN. The results of these experiments revealed that a drug solvent with viscosity ranges from 427 to 8,020 mPa-s would not be suitable for the clinical administration of drugs using the LDDS.

On CT images, the lymphatic vessels from the SiLN to PALN could not be seen after administration of a contrast agent alone (817 kPa, 1 mPa-s) into the SiLN (Table S3). However, when solution F (1,897 kPa, 11 mPa-s) was administered to the SiLN followed by administration of the contrast agent into the SiLN, the dilated

lymphatic vessels between the SiLN and PALN were clearly visualized (Figure 1b).

Next, Indian ink alone (4 mPa-s) (Table S3), solution C (695 kPa, 2 mPa-s) + Indian ink, solution D (1,140 kPa, 4 mPa-s) + Indian ink, and solution J (2,780 kPa, 38 mPa-s) + Indian ink was administered into the SiLN of the respective mouse, and the macroscopical distribution of the Indian ink in the SiLN and the PALN was evaluated 5 min after administration (Figure 2). In the PALN of mice, to which only Indian ink was administered into the SiLN, a small amount of Indian ink was observed in the lymphatic sinuses, but almost no Indian ink was delivered to the LN parenchyma. However, in the PALN of mice to which solutions solution C (695 kPa, 2 mPa-s) + Indian ink, solution D (1,140 kPa, 4 mPa-s) + Indian ink, and solution J (2,780 kPa, 38 mPa-s) + Indian ink administration was followed by Indian ink into the SiLN, Indian ink was observed in the lymphatic sinus and LN parenchyma. The distribution of ink within the PALN was more widespread using solution C (695 kPa, 2 mPa-s) + Indian ink and solution D (1,140 kPa, 4 mPa-s) + Indian ink than when using solution J (2,780 kPa, 38 mPa-s) + Indian ink. The lymphatic vessels connecting the SiLN and PALN were more

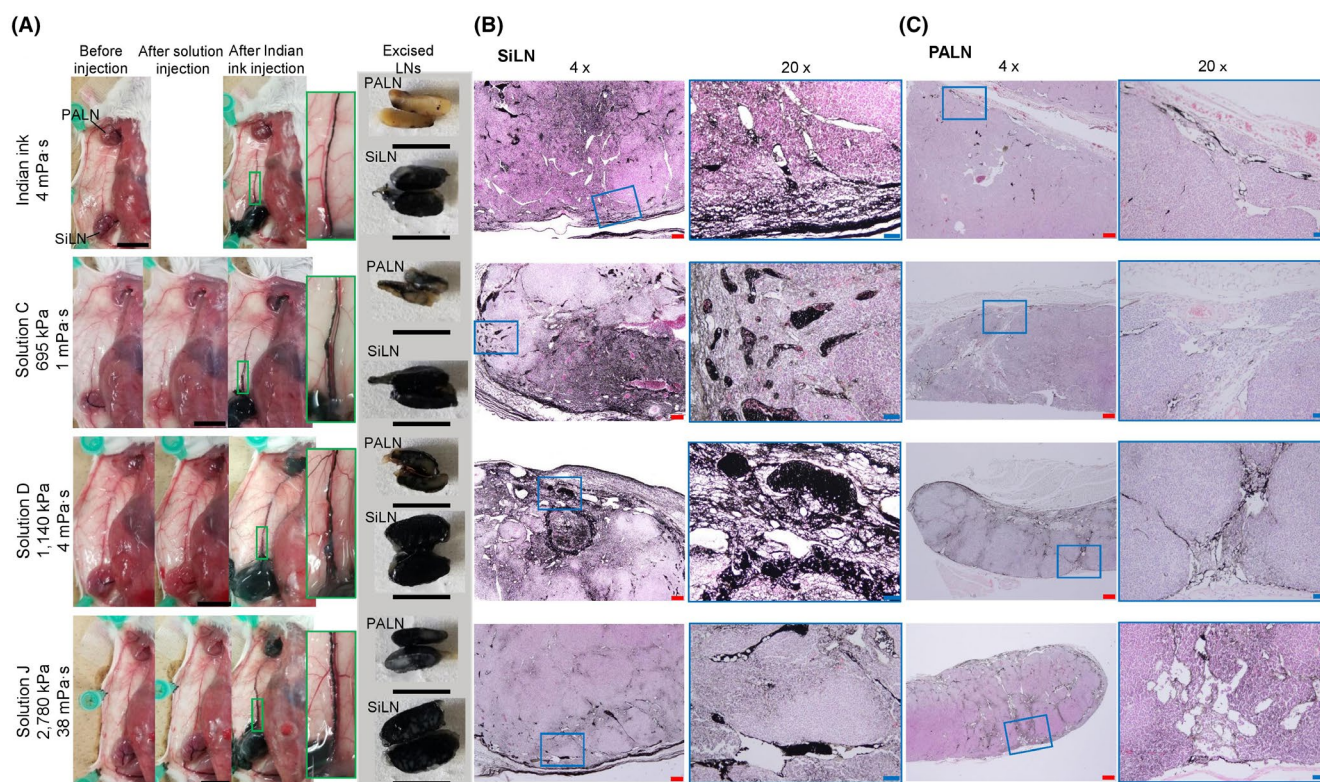


FIGURE 2 Lymphatic vessel visualization and distribution of molecules in the proper axillary lymph nodes (PALN). (a) Two-hundred microliters of test solutions (C, D, J) were injected into the subiliac lymph nodes (SiLN) toward the PALN at an injection rate of 2,400 $\mu\text{L}/\text{min}$ (bolus) after lymphatic and venous systems were exposed surgically. Indian ink was injected 5 min after injection of the high osmotic pressure solution. The flow between the PALN and SiLN was observed. The lymph nodes (LN) were harvested 5 min after Indian ink injection, and hemisected LN photos were taken immediately before paraffin embedding. Lymphatic vessel (LV) expansion was observed in the low to high osmotic pressure solution groups. The distribution of the Indian ink in the PALN increased with increasing osmotic pressure and viscosity. Green boxes in mouse images outline the magnified view of expanded lymphatic vessel. Indian ink (4 mPa-s, $n = 4$), solution C (II: 695 kPa, μ : 2 mPa-s, $n = 4$) + Indian ink, solution D (II: 1,140 kPa, μ : 4 mPa-s, $n = 4$) + Indian ink, solution J (II: 2,780 kPa, μ : 38 mPa-s, $n = 4$) + Indian ink. (b and c) H&E-stained section of PALN (b) and SiLN (c) of a 2.5 μm cut section. Scale bars = 200 μm (red). Boxes in H&E-stained images outline the magnified view of H&E staining. Scale bars = 50 μm (blue)

diluted with solution D (1,140 kPa, 4 mPa·s) + Indian ink and solution J (2,780 kPa, 38 mPa·s) + Indian ink than after administration of solution C (695 kPa, 2 mPa·s) + Indian ink (Figure 2a). Indian ink readily moved into the cortical, medullary, and marginal sinus of the SiLN after its injection into the SiLN. It leaked from the lymphatic sinuses and penetrated the LN parenchyma (Figure 2b). However, there was no significant difference in the Indian ink distribution in the PALN after Indian ink administration alone and solution C (695 kPa, 2 mPa·s) + Indian ink (Figure 2c). In the case of solution D (1,140 kPa, 4 mPa·s) + Indian ink and solution J (2,780 kPa, 38 mPa·s) + Indian ink, Indian ink readily penetrated the cortical and medullary lymphatic sinus of the SiLN. Indian ink leaked from the lymphatic sinus to the LN parenchyma (Figure 2b). Indian ink injected into the SiLN reached the PALN through the lymphatic vessels and was delivered into the cortical and medullary lymphatic sinus of the PALN (Figure 2c). Considering solution retention, reduced edema, body weight changes, and the ease of solution injection, the osmotic pressure and viscosity range for

the LDDS solvents were between solution C (695 kPa, 2 mPa·s) + Indian ink and solution J (2,780 kPa, 38 mPa·s) + Indian ink.

3.2 | Evaluation of the therapeutic effect of docetaxel at optimized osmotic pressure and viscosity ranges on metastatic LNs using lymphatic drug delivery system

Therapeutic effects of the LDDS on the tumor-bearing SiLN were evaluated using an osmotic pressure-adjusted solution containing DTX optimized for LDDS. Tumor growth and invasion patterns in the SiLN varied with the time elapsed from the date of tumor cell inoculation. In the present study, the tumor bearing SiLN on days 7^I (early stage) and 21^I (late-stage) after inoculation were targeted for treatment, where the tumor cell inoculation into the SiLN was defined as day 0^I. Tumor mass formed as small separate foci in the SiLN by day 7^I, whereas separate foci were enlarged in the SiLN at day 21^I (Figure S2a). *Ex vivo*

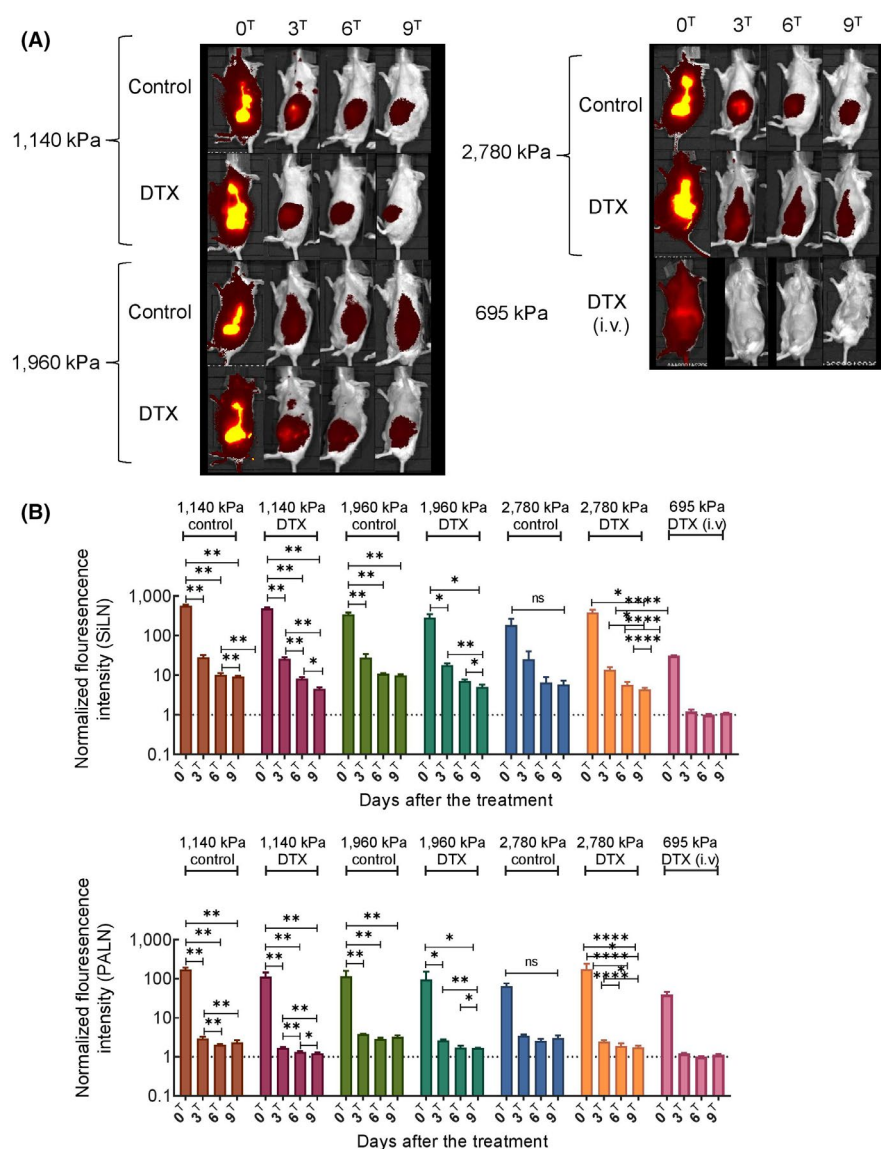


FIGURE 3 Flow dynamics of docetaxel (DTX) solutions between the subiliac lymph nodes (SiLN) and proper axillary lymph nodes (PALN). (a) DTX solution was injected into the SiLN on day 0^T. Flow dynamics were observed on days 0^T (after DTX injection), 3^T, 6^T, and 9^T. Except for 695 kPa DTX (i.v.), solutions were retained in the SiLN and PALN until day 9^T. (b) Fluorescence intensity in the SiLN (upper graph) and PALN (lower graph). Fluorescence values were normalized to those before treatment on 0^T to obtain a normalized fluorescence intensity. Data are given as the mean \pm SEM. Differences between groups were tested by two-way ANOVA and Tukey's post hoc test. ** $P < .01$, *** $P < .001$, **** $P < .0001$. 1,140 kPa control ($n = 6$), 1,960 kPa control ($n = 6$), 2,780 kPa control ($n = 6$), 1,140 kPa DTX ($n = 6$), 1,960 kPa DTX ($n = 5$), 2,780 kPa DTX ($n = 5$), 695 kPa DTX (i.v.) ($n = 6$)

luciferase activity of the SiLN was 10-fold higher on day 21¹ than on day 7¹, and luciferase activity in the SiLN on day 21¹ rapidly increased from day 14¹ after tumor cell inoculation (Figure S2b). LN volume increases were observed on day 7¹ after tumor cell inoculation at day 7¹ and day 21¹, and tumor cell inoculated SiLN volume increased almost onefold in the day 21¹ group (Figure S2b). The ratio of tumor cells in the LN cross-sectional area was 4% at 7¹ and 21¹ days.

Next, we verified the antitumor effect of solutions, which were adjusted to four different osmotic pressures and viscosities and used in the LDDS with and without DTX (Table S4) to treat metastatic LN on day 7¹ (Figure 3). The day when treatment solutions were injected into the SiLN was defined as day 0^T. The fluorescence intensities of SiLN and PALN were increased immediately after treatment (AT) of the DTX solution into the SiLN on day 0^T. The fluorescence intensity decreased to approximately half on day 6 after injection of the treatment solution (Figure 3b). These decreases exhibited similar tendencies, as shown in Figure 1 and Figure S1. Fluorescence intensity in the SiLN and PALN on day 0^T differed between solutions and significant differences were detected in both LN on day 0^T (Figure 3b). However, there was no apparent retention among the solutions in both LN within 3–6 days of treatment. In the i.v. injection group,

retention of DTX solution could not be detected in the SiLN nor in the PALN, except immediately after treatment.

Figure 4 shows the antitumor effects of the solutions on tumors in the SiLN and the PALN as revealed by an *in vivo* bioluminescence imaging system (Figure 4a). In the control groups injected with three different solutions that did not contain DTX and the groups that received DTX i.v. injections, luciferase activity in the SiLN was progressively increased. In these groups, the luciferase activity in the SiLN was approximately 10 to 100-fold higher on day 9^T than on day 0^T (Figure 4b). On the other hand, in the PALN and SiLN in the DTX groups in which DTX solutions with different osmotic pressures and viscosities were injected into the SiLN, luciferase activity was suppressed (Figure 4a,b). These findings suggested that the delivery of drugs with an osmotic pressure and viscosity range (695 kPa, 2 mPa-s–2,780 kPa, 38 mPa-s) that induced lymphatic vasodilatation (Figure 1b and Figure 2a) dramatically improved the antitumor effect.

The LN volumes were measured before the implantation treatment and every experimental day (Figure 5). In mice treated with control solution, regardless of the osmotic pressure, the SiLN volume on day 9^T was three to four times higher than on day 0¹. In contrast, the SiLN volume was little changed or lower on day 9^T (vs day 0¹) in mice

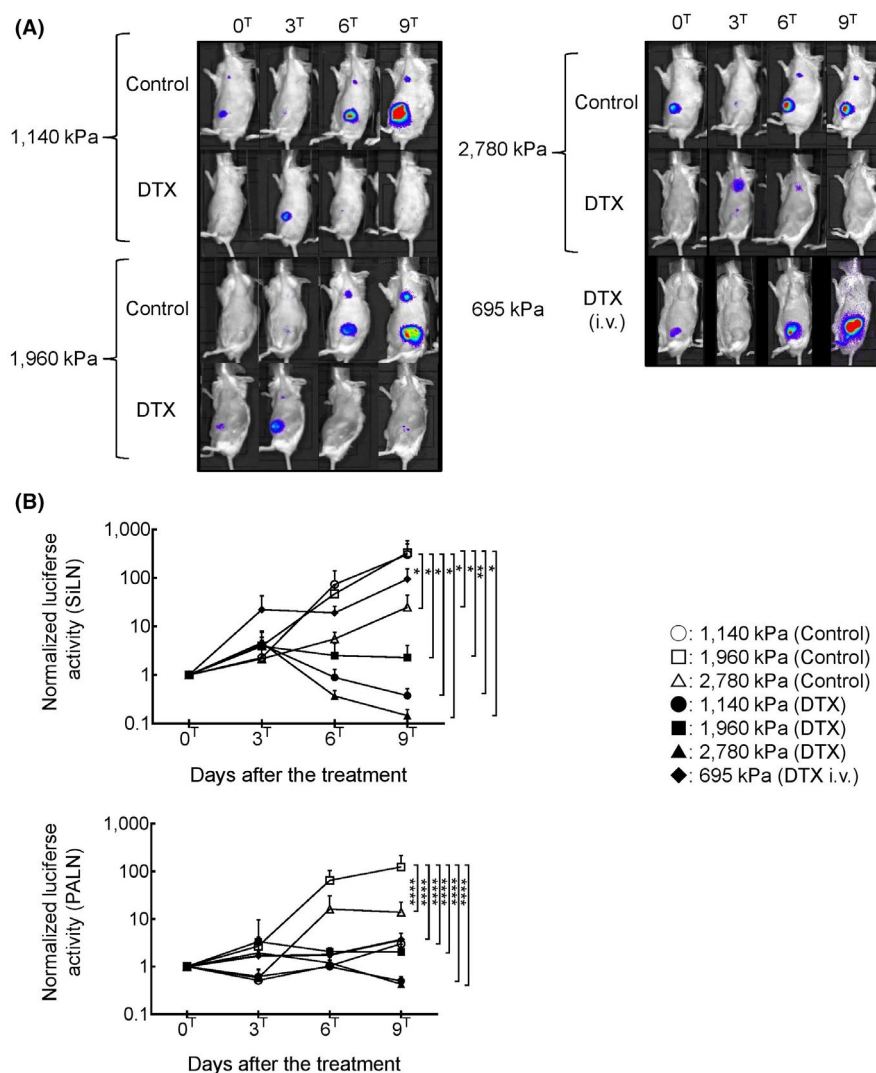


FIGURE 4 Antitumor effects of docetaxel (DTX) solutions at different osmotic pressures in the subiliac lymph nodes (SiLN) and proper axillary lymph nodes (PALN). (a) Bioluminescence (*in vivo*) representative images. Luciferase activity in the SiLN and PALN were measured on days 0^T, 3^T, 6^T, and 9^T. (b) Luciferase activity in the SiLN (upper side) and PALN (lower side) normalized to day 0^T. There were significant differences in luciferase activity in the SiLN and PALN between control and DTX solutions at each osmotic pressure. Data are given as the mean \pm SEM. Differences between groups were tested by two-way ANOVA and Tukey's post hoc test. * $P < .05$. ○, 1,140 kPa control ($n = 6$); □, 1,960 kPa control ($n = 6$); △, 2,780 kPa control ($n = 6$); ●, 1,140 kPa DTX ($n = 6$); ■, 1,960 kPa DTX ($n = 5$); ▲, 2,780 kPa DTX ($n = 5$); ◆, 695 kPa (DTX i.v.) ($n = 6$)

treated with DTX-containing solution (including the DTX i.v. group) (Figure 5a,b). A similar tendency was observed in the PALN; the PALN volume on day 9^T was approximately two times greater than on day 0^I after treatment with DTX-containing solution (Figure 5b).

Figure 6 and Figure 7 shows representative histological data of the SiLN and PALN after treatment with solutions on day 9^T. LN were excised under the same conditions for all groups. Tumor proliferation and invasion along the lymphatic channels were observed in the parenchyma of the SiLN in the control solution groups at 1,140 kPa, 1,960 kPa, and 2,780 kPa (Figure 6a). In some cases, in the SiLN of the control solution groups, tumor proliferation in the marginal sinus and invasion into the efferent lymphatic vessel were detected, while in the PALN of the same groups, tumor invasion from the afferent lymphatic vessels into the marginal sinuses was found (Figure 7a). There were no significant differences in

histological characteristics between tissues examined after control solution injections at different osmotic pressures and viscosities. In the SiLN of groups of mice treated with DTX solutions at different osmotic pressures and viscosities, tumor proliferation and invasion in the parenchyma of the LN, such as those observed in the control groups, were almost entirely replaced by necrotic tissue or dead tumor cells within the lymphatic sinuses. There was no tumor in most areas of the SiLN parenchyma (Figure 6b). In the PALN groups of mice treated with DTX solutions at different osmotic pressures and viscosities, although a small number of tumor cells were observed in the lymphatic channel, these cells showed karyomegaly, karyopyknosis, karyorrhexis, or karyolysis, which suggested a loss of proliferative activity (Figure 7b). Tumor cell proliferation was found after 695 kPa (DTX i.v.) was administered to the SiLN, and tumor cells were found in the parenchyma of its PALN.

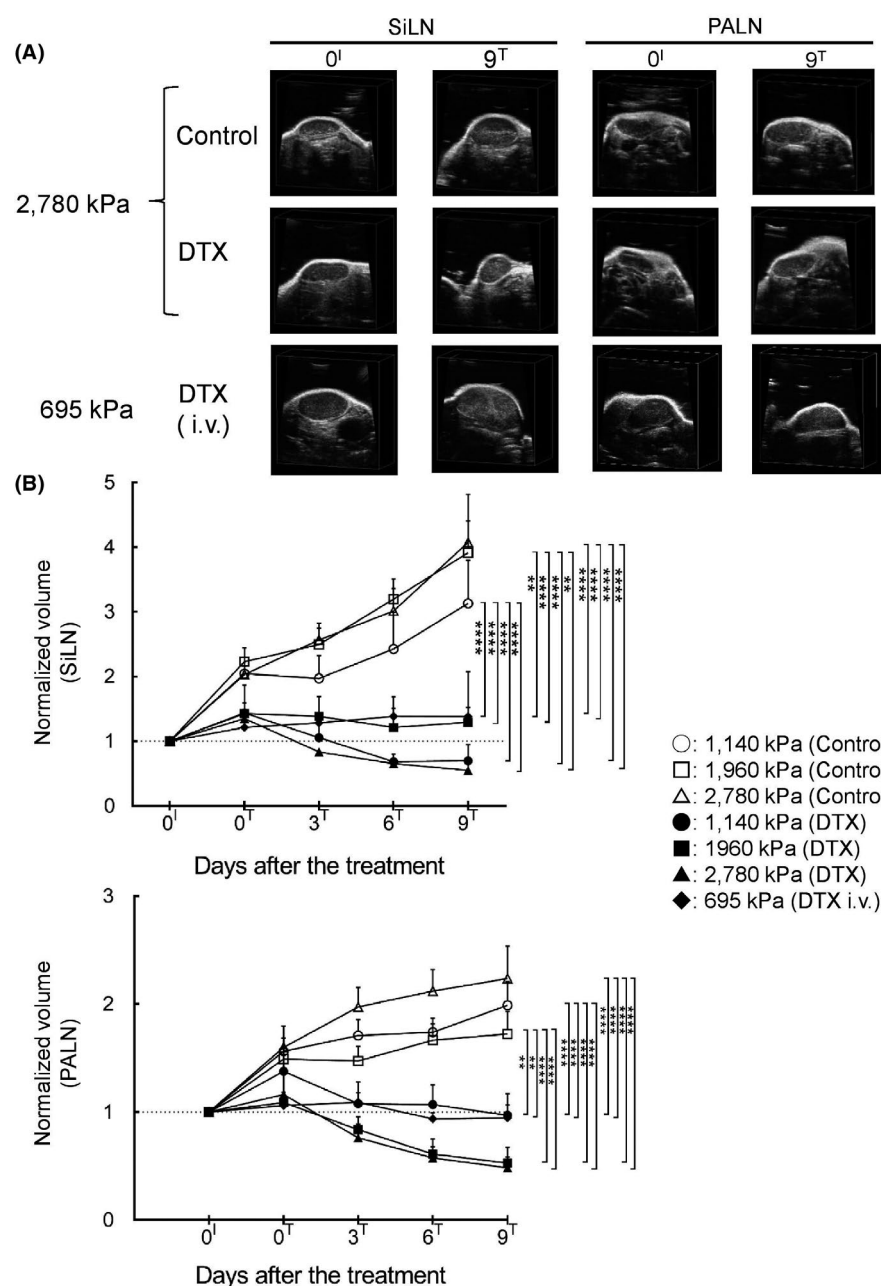
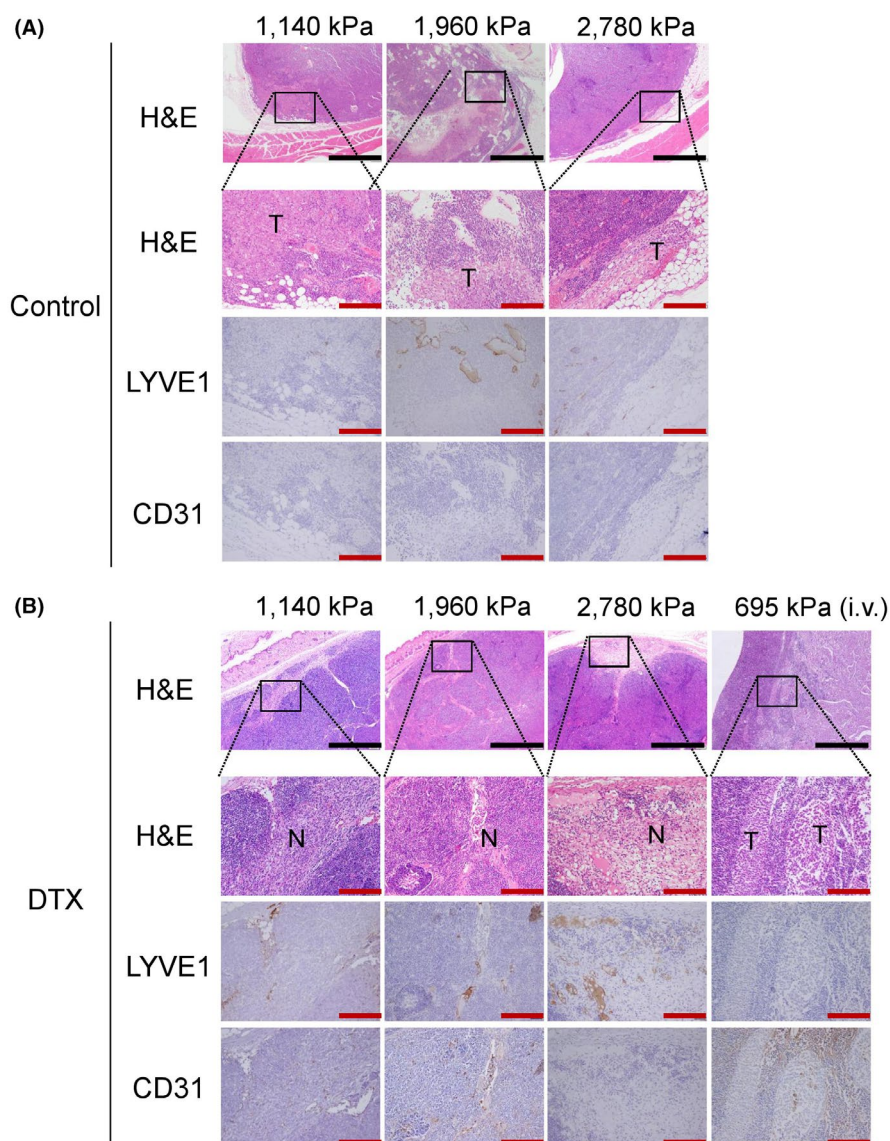


FIGURE 5 Evaluation of the subiliac lymph nodes (SiLN) and proper axillary lymph nodes (PALN) volumes after the injection of solutions at different osmotic pressures. (a) 3D ultrasound representative images of the SiLN and PALN (control and docetaxel (DTX)-containing solutions at 2,780 kPa; 695 kPa DTX i.v.) on day 0^I and day 9^T. (b) SiLN (upper side) and PALN (lower side) volume, normalized to day 0^I, at different times after tumor cell inoculation. Data are given as the mean \pm SEM. Differences between groups were tested by two-way ANOVA and Tukey's post hoc test. * $P < .05$, ** $P < .001$, *** $P < .001$, **** $P < .0001$. ○, 1,140 kPa control ($n = 6$); □, 1,960 kPa control ($n = 6$); △, 2,780 kPa control ($n = 6$); ●, 1,140 kPa DTX ($n = 6$); ■, 1,960 kPa DTX ($n = 5$); ▲, 2,780 kPa DTX ($n = 5$); ◆, 695 kPa (DTX i.v.) ($n = 6$)

FIGURE 6 Histological analyses of the subiliac lymph nodes (SiLN) treated by docetaxel (DTX) solutions at different osmotic pressures. (a) Control. Three solutions with different osmotic pressures. H&E staining and LYVE1 and CD31 immunohistochemistry staining results in the SiLN of a 2.5- μ m section. Scale bars = 1 mm (black). The dotted square was enlarged and analyzed by H&E, LYVE1, and CD31. Scale bars = 200 μ m (red). (b) DTX treatment. H&E and LYVE1 and CD31 immunohistochemistry staining results in the SiLN of a 2.5- μ m section. Scale bars = 1 mm (black). The dotted square was enlarged and analyzed by H&E, LYVE1, and CD31. Scale bars = 200 μ m (red). N, necrosis; T, tumor



In contrast, when the effect of the treatment method was examined from the viewpoint of body weight changes, there were no statistically significant differences for each experimental group (Table S5). We also performed biochemical tests for DTX in the different osmotic pressure groups. No obvious level changes were revealed by the biochemical tests, and there were no statistically significant differences (Table S6).

3.3 | Intranodal delivery of docetaxel at optimized osmotic pressure and viscosity varied with the volume and rate of injection for different stages of metastatic lymph nodes

When we applied the LDDS to treat metastatic LN, differences were detected in the responses to treatments in the metastatic LN between those at an early or advanced stage. Based on previous studies, the LN 7 days after tumor cell inoculation (day 7^l) were defined

as the early metastatic LN model, and the LN 21 days after tumor cell inoculation (days 21^l) defined as the advanced metastatic LN model; experimental treatments were conducted using each metastatic LN model.

Our previous studies⁴³ have shown that when using the LDDS to deliver drugs from upstream to downstream LN, the volume and injection rates of LDDS in the upstream LN dictates the amount of drug delivered to the downstream LN. In the present study, we examined antitumor effects by varying the volume and injection rates into the LN, which were examined on days 7^l and 21^l. A DTX solution with optimized osmotic pressure and viscosity (solution D, 1,140 kPa, 4 mPa·s) was used. The volumes (200 μ L, 400 μ L) and injection rates (200 μ L/min, 2,400 μ L/min) were selected, where 2,400 μ L/min was defined as a bolus rate.^{32,43}

When the DTX solution was injected into the SiLN on different tumor proliferation days with various injection volumes and rates, the solution readily moved from the SiLN to the PALN under these conditions (Figure 8a and Figure 3a), and the flow pattern was similar

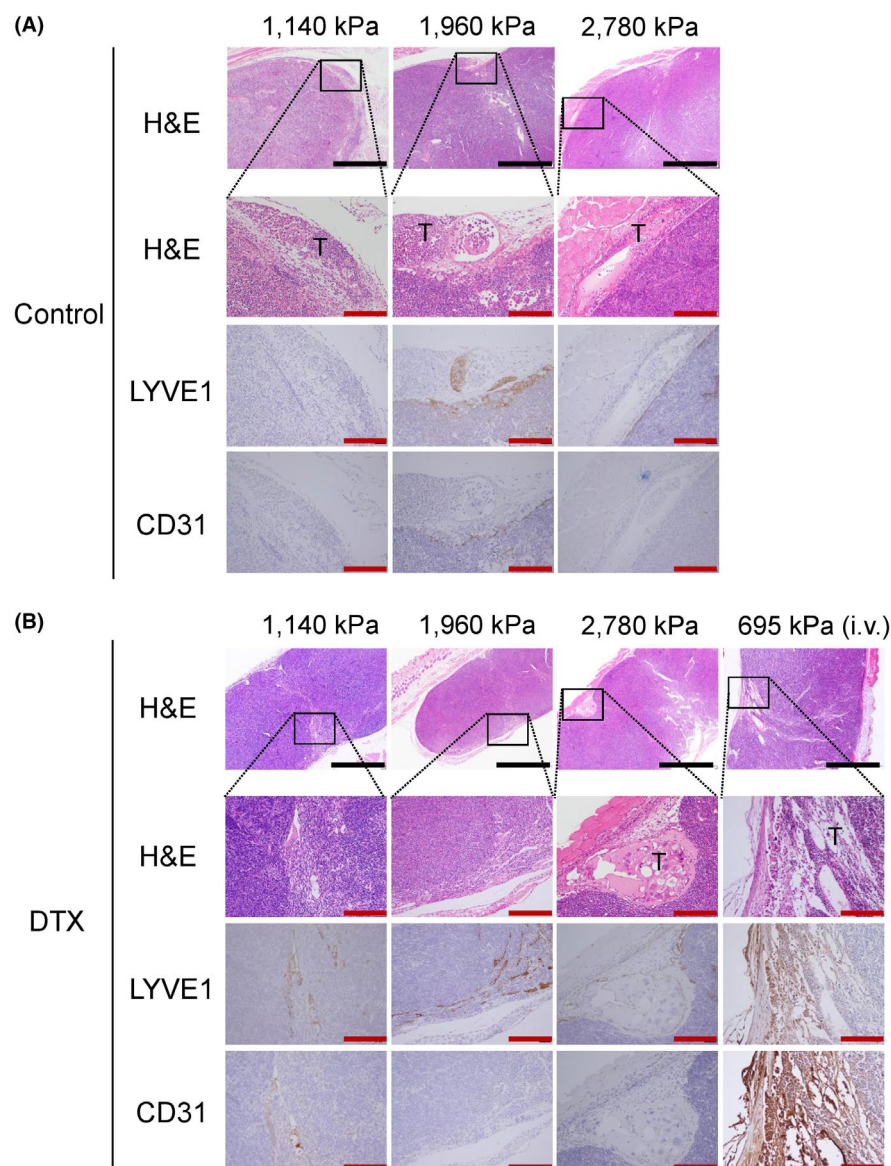


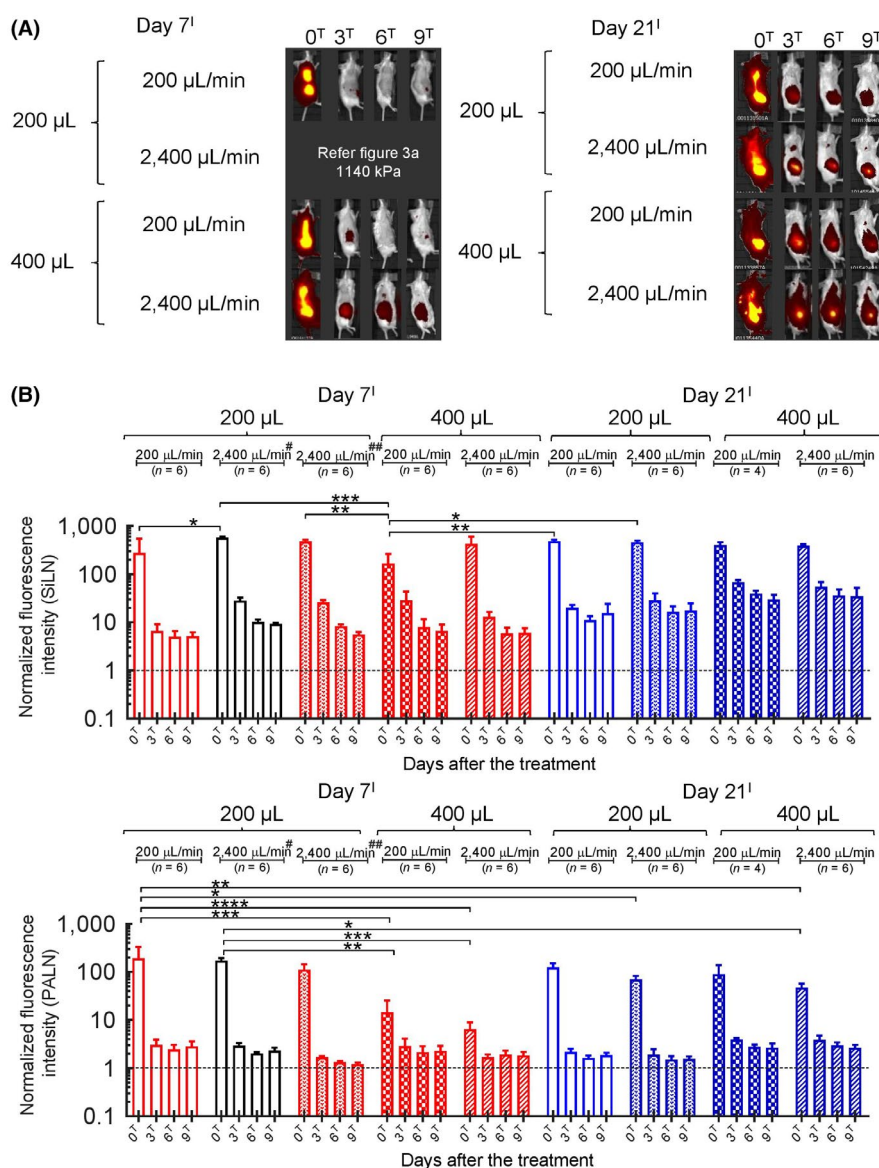
FIGURE 7 Histological analyses of the metastatic proper axillary lymph nodes (PALN) treated by docetaxel (DTX) solutions at different osmotic pressures. (a) Control. Three solutions with different osmotic pressures. H&E staining and LYVE1 and CD31 immunohistochemistry staining results in the PALN of a 2.5- μ m section. Scale bars = 1 mm (black). The dotted square was enlarged and analyzed by H&E, LYVE1, and CD31. Scale bars = 200 μ m (red). (b) DTX treatment. H&E, LYVE1, and CD31 immunohistochemistry staining results in the PALN of a 2.5- μ m section. Scale bars = 1 mm (black). The dotted square was enlarged and analyzed by H&E, LYVE1, and CD31. Scale bars = 200 μ m (red). T, tumor

to that observed in Figure 3. A statistically significant difference in the fluorescence intensity was confirmed immediately after the drug's injection into the SiLN (Figure 8b). The highest fluorescence intensity signal in the SiLN was observed on day 21¹ in the 400 μ L groups. Please refer the data of the 1,140 kPa group in Figure 3a, Figure 4a and Figure 6a for the 200 μ L, 2,400 μ L/min of days 7¹ group indicated in Figure 8a, Figure 9a, and Figure S4a.

Figure 9a shows luciferase activity day 7¹ and day 21¹ treatment results with varied injection volume and rates. Less luciferase activity was detected in the SiLN and PALN after 200 μ L, 2,400 μ L/min on day 7¹, which signaled tumor inhibition. On day 21¹, 400 μ L and 200 μ L/min exhibited the least luciferase activity in the SiLN, and no luciferase activity was detected in the PALN. No significant differences were found in the volume and injection rates that improved the antitumor effect after drug administration into the SiLN on days 7¹ and 21¹ (Figure 9b). Tumor proliferation and invasion were entirely suppressed in the SiLN and PALN on

day 7¹; on day 21¹, slight tumor cell growth inhibition was found (not at a level to suppress tumor proliferation completely). From ultrasound imaging results, tumor cell inoculated SiLN volume was reduced to the same size as the implantation day on day 7¹ after treatment with DTX at 200 μ L or 2,400 μ L/min (bolus) (Figure S3a). Conversely, the tumor cell inoculated SiLN volume was not reduced on day 21¹ after treatment with DTX at 400 μ L or 200 μ L/min. In these experiments, we observed temporary edema around the SiLN into which treatment solutions were injected at the following volumes and rates: 200 μ L, 200 μ L/min; 400 μ L, 200 μ L/min and 400 μ L, 2,400 μ L/min groups for day 7¹; and all groups on day 21¹. Regarding the suppression of tumor growth in the LN, statistically significant differences were found in the SiLN between the groups in the day 7¹ and day 21¹ groups, and increasing volume of the LN was observed on day 21¹ (Figure S3b). No noticeable volume changes were observed in the PALN of all groups; therefore, statistically significant differences were not found in the PALN

FIGURE 8 Flow dynamics of optimized osmotic pressure docetaxel (DTX) solutions administered to the subiliac lymph nodes (SiLN) and proper axillary lymph nodes (PALN) at different injection rates and viscosity ranges. Please refer the data of the 1,140 kPa group in Figure 3a for 200- μ L, 2,400 μ L/min of days 7^I group. (a) DTX solution (1,140 kPa) was injected into the SiLN on day 0^T. Flow dynamics were observed on days 0^T (after DTX injection), 3^T, 6^T, and 9^T. All solutions were retained in the SiLN until day 9^T. (b) Fluorescence intensity in the SiLN (upper graph) and PALN (lower graph). Fluorescence values were normalized to those before treatment on 0^T (before DTX solution injection on day 7^I and/or day 21^I) to obtain a normalized fluorescence intensity. Data are given as the mean \pm SEM. Differences between groups were tested by two-way ANOVA and Tukey's post hoc test. * $P < .05$, ** $P < .01$, *** $P < .001$, **** $P < .0001$



between the day 7^I and day 21^I groups. In the histological analyses, tumor cells were found located in the parenchyma and marginal sinus of the SiLN of the 200 μ L day 7^I group, excluding the 2,400 μ L/min group (Figure S4a). For the 200 μ L and 2,400 μ L/min group on day 7^I, tumor cells were replaced with necrotic tissue. On the other hand, extranodal and intranodal tumor invasion was found for SiLN on day 21^I, with the exception of the 400 μ L and 200 μ L/min treated group (Figure S4b). There were no statistically significant differences in mouse body weight during the study between groups (Table S7).

4 | DISCUSSION

Our study produced four significant findings. First, the optimal osmotic pressure range of LDDS solutions for the treatment of metastatic LN is 695–2,780 kPa; for viscosity, it is <40 mPa·s (Figures 1 and 2 and Figure S1). Up to this viscosity value, the macroscopic

flow dynamics of the drug did not significantly differ. Second, the lymphatic vessels from the SiLN to the PALN and lymphatic channels were dilated in the optimal osmotic range, and the drug was delivered into the parenchyma of the LN (Figure 4). Third, for early (day 7^I) and late (day 21^I) metastatic LN, LDDS applied chemotherapeutic agents showed antitumor effects against the SiLN and PALN. For late metastatic LN (day 21^I), the dose volume (400 μ L) and rate of administration (200 μ L/min) showed significant antitumor effects (Figure 9). Fourth, severe adverse effects were not observed after administering the optimal solution (Figure 5, Figure S2, Table S5, Table S6, and Table S7).

Drug efficacy depends on drug bioavailability, solubility, selection of an appropriate delivery system, and an appropriate administration route. Conventional treatments for metastatic LN include subcutaneous administration,⁴⁴ intraperitoneal administration,⁴⁵ and oral administration^{32,46} of antitumor molecules delivered into the lymphatic system to treat metastatic LN, even though multiple SLN exist around the primary lesion.^{32,47} For clinical use of an

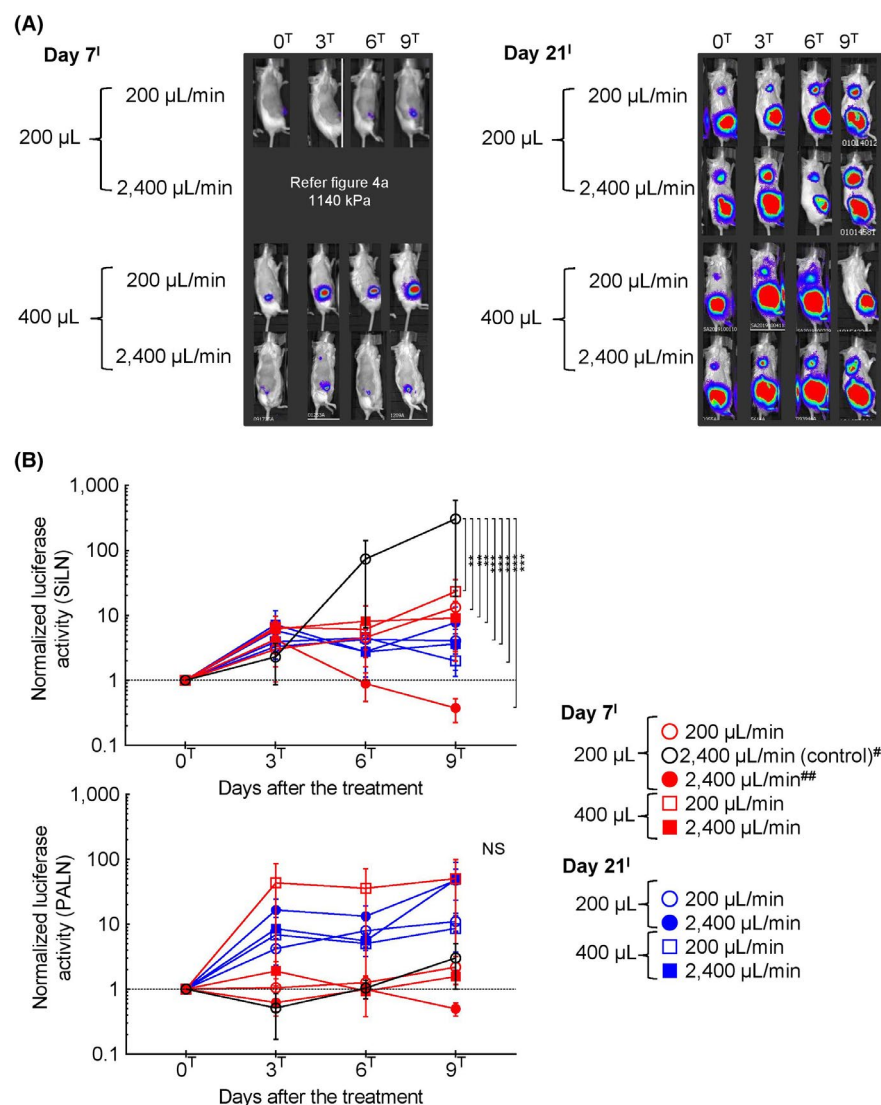


FIGURE 9 Antitumor effects of optimized osmotic pressure solutions of docetaxel (DTX) using different injection rates/viscosity ranges in the subiliac lymph nodes (SiLN) and proper axillary lymph nodes (PALN). Please refer the data of 1,140 kPa group in Figure 4a for 200 μ L 2,400 μ L/min of days 7^I group. (a) Bioluminescence (in vivo) representative images. Luciferase activities in the SiLN and PALN were measured on days 0^T, 3^T, 6^T, and 9^T. (b) Luciferase activity in the SiLN (upper side) and PALN (lower side) normalized to day 0^T. There were significant differences in luciferase activity in the SiLN between D7^I 200 μ L 2,400 μ L/min (control)[#] and DTX solutions at each injection rate/volume range. No significant difference was observed in the luciferase activity of the PALN. Data are given as the mean \pm SEM. Differences between groups were tested by two-way ANOVA and Tukey's post hoc test. ** $P < .01$, *** $P < .001$. ○, D7^I, 200 μ L, 200 μ L/min, $n = 6$; ○, D7^I, 200 μ L 2,400 μ L/min (control)[#], $n = 6$; ●, D7^I, 200 μ L, 2,400 μ L/min^{##}, $n = 6$; □, D7^I, 400 μ L, 200 μ L/min, $n = 6$; ■, D7^I, 400 μ L, 2,400 μ L/min, $n = 6$; ○, D21^I, 200 μ L, 200 μ L/min, $n = 6$; ●, D21^I, 200 μ L, 2,400 μ L/min, $n = 6$; □, D21^I, 400 μ L 200 μ L/min, $n = 6$; ■, 21^I, 400 μ L 2,400 μ L/min, $n = 6$

LDDS, from a technical point of view, the regional LN, which can be detected by ultrasound imaging, will receive the drug. From the pathological point of view, LN at the level of intramodular invasion would be selected for LDDS, and all injectable LN downstream of the tumor draining LN would be selected for treatment.^{29,32} When hyperosmotic fluid was injected into the SLN, it was assumed that blood components would flow out of blood vessels and high endothelial venules (HEV)^{32,48} to reduce the osmotic pressure in the SLN. In addition, high osmotic fluid flows in the efferent lymphatic vessels. Lymphatic vessels are bound to the surrounding extracellular matrix via anchoring filaments^{32,49} containing fibrillin.^{32,50,51} When the osmotic pressure in the lymphatic vessels increases, the anchoring filaments promote the opening of the interendothelial gap and the lymphatic vessels dilate as fluid from the interstitium, macromolecules, and cells flow into the lymphatic vessels. Due to the dilation of lymphatic channels and vessels, hyperosmotic lysates cover tumor cells growing in these pathways, resulting in the delivery of chemotherapeutic agents into tumor cells by passive diffusion.

As shown in a previous study, we found that the optimal ranges of osmotic pressure were greater than for saline and $<3,000$ kPa.³⁶ The optimal conditions of osmotic pressure and viscosity presented in this study were not limited to DTX. In the LDDS, a solvent with an osmotic pressure and viscosity of 1,960 kPa and 12 mPa·s would be appropriate. These values would apply to most of the drugs currently used in systemic chemotherapy and also for repurposed and newly developed chemotherapeutic agents. This technique would be independent of the intra-tumor heterogeneity that is a problem with marker-based antitumor treatments. Conventional drugs, due to their high lipophilicity and low water solubility,^{32,52} are solubilized with high concentrations of surfactants and co-solvents, thus inducing side effects.

In the present study, a single dose of DTX at 10 mg/kg administered using the LDDS was sufficient to achieve an antitumor effect, and there were no noticeable side effects. However, this dose is much smaller than the total dose of 20–116 mg/kg^{32,53} of DTX administered multiple times to treat solid tumors of different tumor types in nude mice. In our study, the maximum osmotic

pressure was assumed to be 3,000 kPa (40 mPa·s), and edema was likely to occur around the LN above this level. Although edema was localized and does not represent a functional impairment of the body, such as a postoperative disfunction associated with LN dissection, local edema around the LN needs to be investigated in clinical practice.

Currently, the clinical significance of LN dissection is debated based on survival data, regardless of the tumor type.^{32,54-57} Our group has proposed the LN-mediated hematogenous metastasis theory^{18,19,32,58} and argued that during LN metastasis at the early stage, tumor cells metastasize systemically via blood vessels. Studies related to this theory have been published recently.^{32,59,60} In addition, our research group has shown that LN dissection induces activation of tumor cells that have metastasized to distant organs.^{32,39,41,42}

In summary, the rationale for LDDS targeting metastatic LN is to treat tumor tissue within metastatic LN, prevent distant metastasis of tumor cells from metastatic LN, avoid vascular damage, nerve damage, incisional infection, lymphedema^{32,61} associated with LN removal, and the activation of tumor cells in distant organs associated with LN dissection and minimizing side effects. Therefore, the injection duration of chemotherapy drugs using the LDDS will be less than for the intratumoral or intralesion methods used in the clinic, and systemic toxicity will be less than for tumor-targeted therapy or systemic chemotherapy. Moreover, administrable drugs in this novel method of ultrasound-guided LDDS or LDDS at intraoperative or image-guided surgery are not limited to chemotherapeutic agents. This method can use a wide range of other types of injections and infusions, such as antitumor vaccines, immune-checkpoint inhibitors, and cytokines at lower concentrations compared to optimal biological doses of those with a higher accumulation in the target area over a short period of time. Ultrasound-guided LDDS can be used in outpatient clinics without hospitalization immediately after the primary tumor has been identified. In cases of LDDS use during intraoperative or image-guided surgery, the advantages are real-time feedback with precise intervention, greater control of the area of SLN (tumor area), and being less invasive than other cancer metastasis therapies.

Advances in the understanding of immune modulation have led to the development of various new therapies to treat and prevent diseases such as cancer metastasis, immune disorders, metabolic disorders, infections, and allergies. Immunotherapy requires the engagement of immune cells, including antigen-presenting cells such as B cells, T cells, and dendritic cells, which are heterogeneously distributed throughout the body and concentrated in specific areas of the LN and lymphoid organs, but they are not easily accessible by systemic administration.

In the future, optimizing factors, such as particle size, molecular weight, surface charge, lipophilicity, concentration, and the surface modification of biomaterials^{32,46} to provide optimal osmolality and viscosity, will enable immunological strategies that can efficiently deliver biomaterials to these immune cells. For clinical translation, lymph drainage processes and LN structures appear to be similar across species, highlighting the relevance of animal studies.



ACKNOWLEDGMENTS

Supported in part by JSPS KAKENHI grant numbers 18H03544 to MS; 20K20161 to SA; 17K20077, 17H00865, 19K22941, and 20H00655 to KT. T. Sato and the Tohoku University Graduate School of Medicine's Biomedical Research Core provided technical assistance and support to the authors.

CONFLICT OF INTEREST

Yakult Honsha provided commercial research support to TK. There were no conflicts of interest among the other authors.

ORCID

Ariunbuyan Sukhbaatar  <https://orcid.org/0000-0001-9137-2966>
Tetsuya Kodama  <https://orcid.org/0000-0003-4727-9558>

REFERENCES

1. Tateda M, Shiga K, Yoshida H, et al. Management of the patients with hypopharyngeal cancer: eight-year experience of Miyagi Cancer Center in Japan. *Tohoku J Exp Med*. 2005;205:65-77.
2. Shiga K, Ogawa T, Kobayashi T, et al. Malignant melanoma of the head and neck: A multi-institutional retrospective analysis of cases in northern Japan. *Head Neck*. 2012;34:1537-1541.
3. Permana AD, Nainu F, Moffatt K, Larrañeta E, Donnelly RF. Recent advances in combination of microneedles and nanomedicines for lymphatic targeted drug delivery. *Wiley Interdiscip Rev Nanomed Nanobiotechnol*. 2021;13:e1690.
4. Oussoren C, Zuidema J, Crommelin DJ, Storm G. Lymphatic uptake and biodistribution of liposomes after subcutaneous injection. II. Influence of liposomal size, lipid composition and lipid dose. *Biochim Biophys Acta*. 1997;1328:261-272.
5. Oussoren C, Storm G. Lymphatic uptake and biodistribution of liposomes after subcutaneous injection: III. Influence of surface modification with poly(ethyleneglycol). *Pharm Res*. 1997;14:1479-1484.
6. Reddy ST, Rehor A, Schmoekel HG, Hubbell JA, Swartz MA. In vivo targeting of dendritic cells in lymph nodes with poly(propylene sulfide) nanoparticles. *J Control Release*. 2006;112:26-34.
7. Reddy ST, Berk DA, Jain RK, Swartz MA. A sensitive in vivo model for quantifying interstitial convective transport of injected macromolecules and nanoparticles. *J Appl Physiol*. 1985;2006:1162-1169.
8. Porter CJH, Trevaskis NL. Targeting immune cells within lymph nodes. *Nat Nanotechnol*. 2020;15:423-425.
9. Rincon-Restrepo M, Mayer A, Hauert S, et al. Vaccine nanocarriers: Coupling intracellular pathways and cellular biodistribution to control CD4 vs CD8 T cell responses. *Biomaterials*. 2017;132:48-58.
10. Schudel A, Francis DM, Thomas SN. Material design for lymph node drug delivery. *Nat Rev Mater*. 2019;4:415-428.
11. Trevaskis NL, Kaminskas LM, Porter CJ. From sewer to saviour – Targeting the lymphatic system to promote drug exposure and activity. *Nat Rev Drug Discov*. 2015;14:781-803.
12. Gretz JE, Norbury CC, Anderson AO, Proudfoot AE, Shaw S. Lymph-borne chemokines and other low molecular weight molecules reach high endothelial venules via specialized conduits while a functional barrier limits access to the lymphocyte microenvironments in lymph node cortex. *J Exp Med*. 2000;192:1425-1440.
13. Cao E, Lindgren A, Martinsson S, et al. Promoting intestinal lymphatic transport targets a liver-X receptor (LXR) agonist (WAY-252,623) to lymphocytes and enhances immunomodulation. *J Control Release*. 2019;296:29-39.
14. Sixt M, Kanazawa N, Selg M, et al. The conduit system transports soluble antigens from the afferent lymph to resident dendritic cells in the T cell area of the lymph node. *Immunity*. 2005;22:19-29.

15. Liu H, Moynihan KD, Zheng Y, et al. Structure-based programming of lymph-node targeting in molecular vaccines. *Nature*. 2014;507:519-522.
16. Zgair A, Lee JB, Wong JCM, et al. Oral administration of cannabis with lipids leads to high levels of cannabinoids in the intestinal lymphatic system and prominent immunomodulation. *Sci Rep*. 2017;7:14542.
17. Kelch ID, Bogle G, Sands GB, Phillips AR, LeGrice IJ, Dunbar PR. Organ-wide 3D-imaging and topological analysis of the continuous microvascular network in a murine lymph node. *Sci Rep*. 2015;5:16534.
18. Kodama T, Mori S, Nose M. Tumor cell invasion from the marginal sinus into extranodal veins during early-stage lymph node metastasis can be a starting point for hematogenous metastasis. *J Cancer Metastasis Treat*. 2018;4:56.
19. Takeda K, Mori S, Kodama T. Study of fluid dynamics reveals direct communications between lymphatic vessels and venous blood vessels at lymph nodes of mice. *J Immunol Methods*. 2017;445:1-9.
20. Yamaki T, Sukhbaatar A, Mishra R, et al. Characterizing perfusion defects in metastatic lymph nodes at an early stage using high-frequency ultrasound and micro-CT imaging. *Clin Exp Metastasis*. 2021;38:539-549. 10.1007/s10585-021-10127-6
21. Jeong HS, Jones D, Liao S, et al. Investigation of the lack of angiogenesis in the formation of lymph node metastases. *J Natl Cancer Inst*. 2015;107:1-11.
22. Mikada M, Sukhbaatar A, Miura Y, et al. Evaluation of the enhanced permeability and retention effect in the early stages of lymph node metastasis. *Cancer Sci*. 2017;108:846-852.
23. Iwamura R, Sakamoto M, Mori S, Kodama T. Imaging of the mouse lymphatic sinus during early stage lymph node metastasis using intranodal lymphangiography with X-ray micro-computed tomography. *Mol Imaging Biol*. 2019;21:825-834. 10.1007/s11307-018-01303-4
24. Cabral H, Makino J, Matsumoto Y, et al. Systemic targeting of lymph node metastasis through the blood vascular system by using size-controlled nanocarriers. *ACS Nano*. 2015;9:4957-4967.
25. Shao L, Mori S, Yagishita Y, et al. Lymphatic mapping of mice with systemic lymphoproliferative disorder: Usefulness as an inter-lymph node metastasis model of cancer. *J Immunol Methods*. 2013;389:69-78.
26. Nose M, Komori H, Miyazaki T, Mori S. Genomics of vasculitis: lessons from mouse models. *Ann Vasc Dis*. 2013;6:16-21.
27. Li L, Mori S, Kodama M, Sakamoto M, Takahashi S, Kodama T. Enhanced sonographic imaging to diagnose lymph node metastasis: importance of blood vessel volume and density. *Can Res*. 2013;73:2082-2092.
28. Li L, Mori S, Sakamoto M, Takahashi S, Kodama T. Mouse model of lymph node metastasis via afferent lymphatic vessels for development of imaging modalities. *PLoS One*. 2013;8:e55797.
29. Kodama T, Matsuki D, Tada A, Takeda K, Mori S. New concept for the prevention and treatment of metastatic lymph nodes using chemotherapy administered via the lymphatic network. *Sci Rep*. 2016;6:32506.
30. Kodama T, Hatakeyama Y, Kato S, Mori S. Visualization of fluid drainage pathways in lymphatic vessels and lymph nodes using a mouse model to test a lymphatic drug delivery system. *Biomedical Optics Express*. 2015;6:124-134.
31. Hansen KC, D'Alessandro A, Clement CC, Santambrogio L. Lymph formation, composition and circulation: A proteomics perspective. *Int Immunol*. 2015;27:219-227.
32. Ito K, Noro K, Yanagisawa Y, et al. High-accuracy ultrasound contrast agent detection method for diagnostic ultrasound imaging systems. *Ultrasound Med Biol*. 2015;41:3120-3130.
33. Tada A, Horie S, Mori S, Kodama T. Therapeutic effect of cisplatin given with a lymphatic drug delivery system on false-negative metastatic lymph nodes. *Cancer Sci*. 2017;108:2115-2121.
34. Fujii H, Horie S, Sukhbaatar A, et al. Treatment of false-negative metastatic lymph nodes by a lymphatic drug delivery system with 5-fluorouracil. *Cancer Med*. 2019;8:2241-2251.
35. Sato T, Mori S, Arai Y, Kodama T. The combination of intralymphatic chemotherapy with ultrasound and nano-/microbubbles is efficient in the treatment of experimental tumors in mouse lymph nodes. *Ultrasound Med Biol*. 2014;40:1237-1249.
36. Fukumura R, Sukhbaatar A, Mishra R, Sakamoto M, Mori S, Kodama T. Study of the physicochemical properties of drugs suitable for administration using a lymphatic drug delivery system. *Cancer Sci*. 2021;112:1735-1745. 10.1111/cas.14867
37. Komori H, Terada M, Ito MR, et al. Genetic Dissection of autoimmune disease phenotypes in a new recombinant inbred strain of mice MXH/lpr. *Tissue Antigens*. 2004;64:402-403.
38. Van den Broeck W, Derore A, Simoons P. Anatomy and nomenclature of murine lymph nodes: Descriptive study and nomenclature standardization in BALB/cAnNCrl mice. *J Immunol Methods*. 2006;312:12-19.
39. Shao L, Ouchi T, Sakamoto M, Mori S, Kodama T. Activation of latent metastases in the lung after resection of a metastatic lymph node in a lymph node metastasis mouse model. *Biochem Biophys Res Comm*. 2015;460:543-548.
40. Ouchi T, Sukhbaatar A, Horie S, et al. Superselective drug delivery using doxorubicin-encapsulated liposomes and ultrasound in a mouse model of lung metastasis activation. *Ultrasound Med Biol*. 2018;44:1818-1827.
41. Zheng J, Jia L, Mori S, Kodama T. Evaluation of metastatic niches in distant organs after surgical removal of tumor-bearing lymph nodes. *BMC Cancer*. 2018;18:608.
42. Sukhbaatar A, Mori S, Saiki Y, Takahashi T, Horii A, Kodama T. Lymph node resection induces the activation of tumor cells in the lungs. *Cancer Sci*. 2019;110:509-518.
43. Fujii H, Horie S, Takeda K, Mori S, Kodama T. Optimal range of injection rates for a lymphatic drug delivery system. *J Biophotonics*. 2018;11:e201700401.
44. Porter CJ, Charman SA. Lymphatic transport of proteins after subcutaneous administration. *J Pharm Sci*. 2000;89:297-310.
45. Sugarbaker PH, Stuart OA. Intraperitoneal doxorubicin achieves access to mesenteric lymph nodes, case series of two patients. *Int J Surg Case Rep*. 2019;54:108-112.
46. Vishwakarma N, Jain A, Sharma R, Mody N, Vyas S, Vyas SP. Lipid-based nanocarriers for lymphatic transportation. *AAPS PharmSciTech*. 2019;20:83.
47. Zhang C, Zhang L, Xu T, et al. Mapping the spreading routes of lymphatic metastases in human colorectal cancer. *Nat Commun*. 2020;11:1993.
48. Girard JP, Moussion C, Forster R. HEVs, lymphatics and homeostatic immune cell trafficking in lymph nodes. *Nat Rev Immunol*. 2012;12:762-773.
49. Leak LV, Burke JF. Fine structure of the lymphatic capillary and the adjoining connective tissue area. *Am J Anat*. 1966;118:785-809.
50. Gerli R, Solito R, Weber E, Agliano M. Specific adhesion molecules bind anchoring filaments and endothelial cells in human skin initial lymphatics. *Lymphology*. 2000;33:148-157.
51. Ohtani O, Ohtani Y. Recent developments in morphology of lymphatic vessels and lymph nodes. *Ann Vasc Dis*. 2012;5:145-150.
52. Narvekar M, Xue HY, Eoh JY, Wong HL. Nanocarrier for poorly water-soluble anticancer drugs—barriers of translation and solutions. *AAPS PharmSciTech*. 2014;15:822-833.
53. Bissery MC, Nohynek G, Sanderink GJ, Lavelle F. Docetaxel (Taxotere): A review of preclinical and clinical experience. Part I: Preclinical experience. *Anticancer Drugs*. 1995;6:333-338.
54. Krag DN, Anderson SJ, Julian TB, et al. Sentinel-lymph-node resection compared with conventional axillary-lymph-node dissection in clinically node-negative patients with breast cancer: Overall

- survival findings from the NSABP B-32 randomised phase 3 trial. *Lancet Oncol.* 2010;11:927-933.
55. Ha MH, Choi MG, Sohn TS, Bae JM, Kim S. Prognostic significance of suprapancreatic lymph nodes and its implication on D2 dissection. *Medicine (Baltimore).* 2018;97:e11092.
56. Saito R, Kawaguchi Y, Akaike H, et al. Prognostic significance of lymph node dissection along the upper-third-stomach in patients with lower-third gastric cancer. *Anticancer Res.* 2019;39:1485-1489.
57. Zhang YX, Yang K. Significance of nodal dissection and nodal positivity in gastric cancer. *Transl Gastroenterol Hepatol.* 2020;5:17.
58. Shao L, Takeda K, Kato S, Mori S, Kodama T. Communication between lymphatic and venous systems in mice. *J Immunol Methods.* 2015;424:100-105.
59. Brown M, Assen FP, Leithner A, et al. Lymph node blood vessels provide exit routes for metastatic tumor cell dissemination in mice. *Science.* 2018;359:1408-1411.
60. Pereira ER, Kedrin D, Seano G, et al. Lymph node metastases can invade local blood vessels, exit the node, and colonize distant organs in mice. *Science.* 2018;359:1403-1407.
61. Lyman GH, Temin S, Edge SB, et al. Sentinel lymph node biopsy for patients with early-stage breast cancer: American Society of Clinical Oncology clinical practice guideline update. *J Clin Oncol.* 2014;32:1365-1383.

SUPPORTING INFORMATION

Additional supporting information may be found in the online version of the article at the publisher's website.

How to cite this article: Sukhbaatar A, Mori S, Kodama T. Intranodal delivery of modified docetaxel: Innovative therapeutic method to inhibit tumor cell growth in lymph nodes. *Cancer Sci.* 2022;113:1125-1139. doi:[10.1111/cas.15283](https://doi.org/10.1111/cas.15283)